

***JHK'* Imaging Photometry of Seyfert 1 AGNs and Quasars III:
Variability of Radio Quiet and Radio Loud AGNs**

Keigo Enya¹, Yuzuru Yoshii^{1,4}, Yukiyasu Kobayashi², Takeo Minezaki¹, Masahiro
Suganuma³, Hiroyuki Tomita³ and Bruce A. Peterson⁵

¹ Institute of Astronomy, School of Science, University of Tokyo, Osawa 2-21-1, Mitaka,
Tokyo 181-8588, Japan

² National Astronomical Observatory, Osawa 2-21-1, Mitaka, Tokyo 181-8588, Japan

³ Department of Astronomy, University of Tokyo, Hongo 7-3-1, Bunkyo-ku, Tokyo
113-0033, Japan

⁴ Research Center for the Early Universe (RESCEU), School of Science, University of
Tokyo, Hongo 7-3-1, Bunkyo-ku, Tokyo 113-0033, Japan

⁵ Research School of Astronomy and Astrophysics, The Australian National University,
Weston Creek, ACT 2611, Australia

Received _____; accepted _____

ABSTRACT

Variability of 226 AGNs in the near-infrared J , H , and K' bands is analyzed and discussed. An ensemble average for measured variabilities was obtained for various samples of the AGNs divided by absolute B -magnitude M_B , redshift z , and radio strength. All the samples in the J , H , and K' bands are found to give significant ensemble variability, but no significant wavelength dependence is found. The ensemble variability in the entire sample combining the J , H , and K' samples is $\Delta m \approx 0.22$ mag, while $\Delta m \approx 0.18$ mag for the radio-quiet AGNs and $\Delta m \approx 0.26$ mag for radio-loud AGNs. The ensemble variability for the radio-quiet AGNs shows no significant M_B -dependence, while showing positive M_B -dependence for the radio-loud AGNs. In any samples the measured variability shows positive correlation among different passbands, with the correlation coefficients of r_{JH} , $r_{HK'}$, and $r_{JK'}$ ranging from 0.6 to 0.9. For radio-quiet AGNs, the coefficient $r_{HK'}$ in a redshift range of $0.1 < z < 0.3$ is significantly higher than r_{JH} or $r_{JK'}$. The coefficient for the radio-loud AGNs with $0.6 < z < 1.0$ is as high as 0.95, irrespective of the passband. However, for the radio-quiet AGNs with $z > 0.3$ and radio-loud AGNs with $z < 0.3$, we cannot confirm such strong correlation among different passbands. All the features of near-infrared variability for the radio-quiet AGNs are consistent with a simple dust reverberation model of the central regions of AGNs. However, the features for the radio-loud AGNs are not fully explained by such a model, and a non-thermal variable component is suggested as a viable candidate for causing their large and fast variability in the near-infrared region.

Subject headings: galaxies: active—quasars: general—galaxies: photometry

1. Introduction

Active galactic nuclei (AGNs) at cosmological distance emit enormous amount of energy from their central region which is compact and spacially unresolved. Observations of AGN variability are important for the understanding of the physical mechanisms of energy emission by the central engine.

Monitoring observations of many AGNs in the optical region have been made by various authors, and the relations among AGN optical variability, luminosity, redshift, time scale and so on have been derived. For example, a negative correlation between variability amplitude and luminosity was found, and the possibility of explaining the emission and variability of AGN by a sub-unit model has been discussed (e.g., Cristiani et al. 1996; Hook et al. 1994). The wavelength dependence of variability was discussed by various authors (e.g., Cristiani et al. 1997; Winkler 1997; Winkler et al. 1992). Multi-color monitoring observations of AGNs are useful to distinguish the dependence of variability on wavelength and redshift. Optical variability was compared with ultraviolet variability (Clemente et al. 1996), and it was concluded that the variability was larger in the shorter wavelength UV region than in the optical region.

Further understanding can obviously be made by combining the near-infrared (NIR) data with the UV/optical data. Barvanis (1992) analyzed the optical and NIR light curves of Fairall 9 (Cravel, Wamsterker & Glass 1989), and explained the delay of NIR variability, in terms of a dust reverberation model, in which thermal re-radiation comes from a hot dust torus illuminated by the central emission engine. Neugebauer et al. (1988) monitored 108 PG quasars in the J , H , K , L and $10\mu\text{m}$ bands for about 20 years. It was suggested that the detection rate of variability is smaller in the NIR than in the optical, if the same level of accuracy is required.

We present the new data of J , H , and K' variabilities for 226 AGNs. The sample

was divided into groups by radio strength, absolute B -magnitude, and redshift, and the ensemble variability for each group was measured.

2. Data

Our analysis in this paper was made by using the NIR images of AGNs obtained through the procedure of image reduction discussed in Paper I. Differential photometry was employed to measure their NIR variability. The achieved accuracy was significantly higher than the accuracy from an alternative method of standards-based photometry, as described in Paper II. Only the measurements made with more than two reference objects and having an accuracy higher than 0.1 mag are used in this paper.

The AGNs in our sample were selected from various versions of the Quasars and Active Galactic Nuclei catalog (VV catalog, Veron-Cetty and Veron 1993, 1996, 1998). AGNs were selected with consideration of their use in the MAGNUM Project (Kobayashi et al. 1998a, 1998b). The distribution of declination and right ascension for all AGNs in the sample is shown in Fig. 1 of Paper I. The distribution of absolute B -magnitude and redshift is shown in Fig. 2 of Paper I.

All observations were made with the 1.3m infrared telescope at the Institute of Space and Astronautical Science (ISAS), Japan, equipped with the NIR PICNIC camera (Kobayashi et al. 1994). The AGNs and reference objects were imaged in the J , H and K' bands with the telescope stepped in a raster pattern. Two photometric standard stars with different elevations were observed three times each night (for details see §2 of Paper I).

The PICRED software, that was developed for the PICNIC camera, was used to reduce the images. During our observations this software was optimized for AGN and quasar images, to achieve fully automated reductions (for details see §3 of Paper I).

3. Analysis and Discussion

3.1. ensemble variability

Since each AGN was observed on two different nights separated by a year or more, the variability thus obtained does not necessarily reflect the characteristic amplitude of intrinsic variability. Therefore, we discuss the ensemble variability of AGNs which reflects the dispersion of their individual variabilities. However, the standard deviation of such data is not a good parameter in estimating the AGN variability, because not only the intrinsic AGN variability but also measurement errors broaden the distribution.

We here introduce the ensemble variability, after excluding the contribution of measurement errors, as

$$\Delta m = \sqrt{\frac{\sum_i^N \Delta m_i^2 - \sum_i^N \sigma_i^2}{N}} \quad , \quad (1)$$

and its error given by

$$\sigma_{\Delta m} = \frac{1}{2\Delta m} \sqrt{\frac{\left(\sum_i^N \Delta m_i^2 - \sum \sigma_i^2\right)^2}{N^3} + \frac{\sum_i^N (4\Delta m_i^2 \sigma_i^2 - 2\sigma_i^4)}{N^2}} \quad . \quad (2)$$

Derivation of Δm and $\sigma_{\Delta m}$ is described in Appendix A. In the remainder of this paper these quantities of Δm and $\sigma_{\Delta m}$ are used to discuss the variability of the AGNs in our sample.

3.2. The relation between the variability and AGN character

We examine whether the variability is correlated with the parameters such as radio strength, rest-frame time interval of observations, absolute B -magnitude, redshift, Seyfert type, and NIR colors. First, the sample was divided by each parameter into two groups, “ a ” and “ b ”, at a point where there appeared to be a boundary on either side of which the data are separated. Then, the ensemble variabilities for these two groups were compared with each other.

The AGNs in our sample are distinguished by the radio strength or the ratio of radio 6 cm flux relative to optical V -band flux $f_\nu(6\text{cm})/f_\nu(V)$. The AGNs with $f_\nu(6\text{cm})/f_\nu(V) < 10$ were classified into the radio-quiet group, and others with $f_\nu(6\text{cm})/f_\nu(V) > 100$ into the radio-loud group. The AGNs, observed twice separated by time interval Δt_{obs} , were distinguished by the rest-frame time interval $\Delta t_{\text{rest}} \equiv \Delta t_{\text{obs}}/(1+z)$. The AGNs with 100 days $< \Delta t_{\text{rest}} < 400$ days were classified into the short- Δt_{rest} group, and others with 400 days $< \Delta t_{\text{rest}} < 800$ days into the long- Δt_{rest} group. The boundary at 400 days reflects the period in which the AGNs were observed. Our observational runs consist of three periods (January 1996–April 1996, November 1996–February 1997, December 1997–April 1998). The AGNs observed in the first and third periods are mainly of long interval, and those in the second and third periods are of short interval. The AGNs with $M_B < -23.5$ were classified into the bright group, and those with $M_B > -23.5$ into the faint group. The AGNs with $z < 0.3$ are classified into the low- z group, and those with $z > 0.3$ into the high- z group. The AGNs with Seyfert 1, 1.2, and 1.5 were classified into the early-type Seyfert group, and others with 1.8, 1.9, and 2 into the late-type Seyfert group. The AGNs with $J - H < 0.8$ and those with $H - K' < 0.8$ were classified into the blue group, and others with $J - H > 0.8$ and $H - K' > 0.8$ into the red group.

The ensemble variabilities for the “ a ” and “ b ” groups are derived for each of radio strength, rest-frame time interval of observations, absolute B -magnitude, redshift, Seyfert type, and NIR colors. Table 1 shows the ratio $\Delta m(\text{“}a\text{”})/\Delta m(\text{“}b\text{”})$ for each of the above parameters. The last column of this table represents the average ratio taken over the J , H , and K' bands. The average ratio between the radio-loud and radio-quiet groups is 1.46, which is the largest. The average ratio for the long- and short- Δt_{rest} groups is 1.24, while it is 1.20 for the bright- and faint- M_B groups. The average ratios for other quantities are much closer to unity.

Top panel of Fig. 1 shows that the ensemble variability in the J , H , or K' band is $\Delta m \approx 0.2$, estimated for the entire sample, while $\Delta m \approx 0.25 - 0.3$ and $0.18 - 0.2$ for the radio-quiet and radio-loud groups, respectively. We see no significant wavelength-dependence of Δm .

We divide the radio-quiet or radio-loud group furthermore into two subgroups of short and long Δt_{rest} , and estimate the ensemble variability for respective subgroups. Bottom panels of Fig. 1 show that the ensemble variability in the J , H , or K' band is $\Delta m \approx 0.2$ (long Δt_{rest}) and 0.15 (short Δt_{rest}) for the radio-quiet sample, while $\Delta m \approx 0.28 - 0.32$ (long Δt_{rest}) and $0.22 - 0.28$ (short Δt_{rest}) for the radio-loud sample.

We furthermore divide the short- or long- Δt_{rest} subgroup by M_B or z . In this way, the ensemble variabilities of the radio-quiet AGNs in respective subgroups are shown in Fig. 2. The similar results for the radio-loud AGNs are shown in Fig. 3.

3.2.1. statistical test and estimation of the λ dependence of the ensemble variability

A statistical test on the wavelength dependence of Δm_λ was done by applying the χ^2 method to the result. Since such dependence was not found to be significant, it is reasonable to adopt a two-parameter function of $\Delta m_\lambda(a_1, a_2) = a_1 e^{a_2 \lambda}$ and search for the solution near $a_2 \approx 0$ in minimizing $\chi^2 = \sum_{\lambda=J,H,K'} (\Delta m_\lambda - \Delta m_\lambda(a_1, a_2))^2 / \sigma_{\Delta m_\lambda}^2$. Table 2 shows the optimized values of $a_1 = 0.205$ and $a_2 = 0.029$ for the entire sample, leading to $\Delta m_{K'}/\Delta m_J = 1.03$, otherwise $\Delta m_{K'}/\Delta m_J = 0.83 - 1.26$ (95% C.L.) and $0.79 - 1.32$ (99% C.L.). For the radio-quiet sample, the optimized values of $a_1 = 0.205$ and $a_2 = -0.065$ give $\Delta m_{K'}/\Delta m_J = 0.94$. A similar result holds if the radio-quiet sample is further divided by Δt_{rest} . For other groups, the C.L. range becomes wider, so that the ability of rejecting the hypothesis of no wavelength-dependence by the test remarkably decreases.

3.2.2. statistical dependence test of the ensemble variability on characteristic parameters

In this section, using the ensemble variability Δm averaged over the J , H , and K' bands, we examine whether Δm depends on radio strength, Δt_{rest} , M_B , and z . In this case, with a simple one-parameter function of $\Delta m(a_1) = a_1$, it is reduced to $\chi^2 = \sum_j (\Delta m_j - \Delta m(a_1))^2 / \sigma_{\Delta m_j}^2$. Table 3 shows the optimized value of a_1 together with P which represents the reliability of rejecting the hypothesis that Δm does not depend on the parameter in question.

It is understood from this table that the statistical equivalence of Δm between the radio-quiet and radio-loud samples is rejected by a level of $P \geq 99.9\%$. For the radio-quiet sample further divided by Δt_{rest} , the statistical equivalence of Δm between the short and long Δt_{rest} is also rejected by a level of $P \geq 99.9\%$. For the radio-loud sample, however, such statistical equivalence is rejected only by $P = 71.1\%$.

For the radio-quiet sample with short Δt_{rest} , the test for the M_B -dependence gives $P = 75.0\%$ by which it is difficult to conclude with certainty that Δm depends on M_B . The same test for z -dependence gives $P = 95.5\%$, indicating a rather strong z -dependence of Δm . For the radio-loud sample with short Δt_{rest} , both M_B -dependence and z -dependence are highly significant. We note that such strong M_B -dependence is in clear contrast with the result for the radio-quiet sample, and such strong z -dependence is similar to the result for the radio-quiet sample.

3.2.3. discussion of the parameter dependence of the ensemble variability

Figure 4 shows the relations among various parameters for the radio-quiet sample. In the left column, from top to bottom, are shown the values of Δm , Δt_{rest} , and M_B , estimated in four z -bins between $z = 0$ and 1. Similarly, in the right column, from top to bottom,

are shown the values of Δm , Δt_{rest} , and z , estimated in four M_B -bins between $M_B = -32$ and -18 . In this figure, open and filled squares represent the samples with short and long Δt_{rest} , respectively.

We see from the left column that Δm , Δt_{rest} and M_B decrease with increasing z , except for the case of Δm in the lowest- z bin. These trends with z are equivalently converted to the trends with M_B , as shown in the right column, by using the monotonical z versus M_B relation. We caution that the z -dependence of Δt_{rest} may only be apparent, arising from the cosmological time delay $\Delta t_{\text{rest}} = \Delta t_{\text{obs}}/(1+z)$ applied to our sample which has a rather limited range of Δt_{obs} . Consequently, any trends with Δt_{rest} may also be apparent.

The ensemble NIR variability of radio-quiet AGNs is as small as $\Delta m \leq 0.25$, showing little M_B -dependence in this work. We note that faint AGNs, mostly at low z , are contaminated by a host galaxy component, which is indicated by our multi-aperture color analysis (Paper I; see also Kotilainen & Ward 1994). Since the host galaxy component is stellar and does not vary on a time scale of years, such contamination has the systematic effect of weakening the AGN variability. Therefore, Δm , after correction for this effect, would still have little or negative correlation with absolute B -luminosity, depending on the degree of contamination within chosen aperture size.

The above M_B -dependence of Δm is expected from the model of dust reverberation in which brighter AGNs have a larger dust torus. That is, a variation in the UV/optical light emitted from the central engine is absorbed in more extended region of dust from which the NIR radiation is emitted and the spread in arrival times of the NIR variation from this extended region produces a variation with smaller amplitude. Therefore, regardless of the real emission mechanism of central source, the NIR variability would show only small correlation with M_B , as observed.

Next, we consider the radio-loud AGNs. Figure 5 shows their relations among Δm ,

Δt_{rest} , M_B , and z , in a similar way as in Fig. 4. We divide the radio-loud sample into the short and long Δt_{rest} . However, because of the lack of enough data, the values of Δm and Δt_{rest} are not estimated as a function of z or M_B , for the case of long Δt_{rest} .

We notice that Δm for the radio-loud AGNs, in the case of short Δt_{rest} , strongly increases with increasing z or with increasing absolute B -luminosity, opposite to that for the radio-quiet AGNs. If we assume that such positive correlation is only apparent, wishing to explain it in terms of the effect of contamination of host galaxy component, we have to invoke an extremely different contribution from the host galaxies between radio-loud and radio-quiet AGNs, which is difficult to justify. Therefore, it is more reasonable to conclude that the different M_B -dependence of Δm reflects the different emission and variability mechanisms between radio-loud and radio-quiet AGNs.

3.3. The correlation of variability in different passbands

In this section the correlation among the variabilities in the J , H , and K' bands is discussed using only the data of estimated variabilities with more than two reference stars and an accuracy better than 0.1 mag. The results for the radio-quiet and radio-loud AGNs are shown in Figs. 6 and 7, respectively, where Δm_H is plotted against Δm_J , $\Delta m'_K$ against Δm_H , and $\Delta m'_K$ against Δm_J . Open and filled symbols correspond to long and short Δt_{rest} , respectively.

The data distribute, more or less, along the diagonal running from lower left to upper right through the origin, which indicates that AGNs, becoming brighter in one band, become brighter in the other band, and vice versa. It is seen from each panel that more data are plotted in the lower left region than in the upper right region. However, this is not real because AGNs, becoming fainter, are likely to be either undetected or rejected by our

accuracy requirement.

The correlation coefficient of variabilities in two different bands, say J and H , is defined as

$$r_{JH} = \frac{\sum(\Delta m_{J,i} - \Delta m_J)(\Delta m_{H,i} - \Delta m_H)}{\sqrt{\sum(\Delta m_{J,i} - \Delta m_J)^2 \sum(\Delta m_{H,i} - \Delta m_H)^2}} \quad , \quad (3)$$

where Δm_λ ($\lambda = J$ or H) is the unweighted average of variability data in each band. Table 4 tabulates the values of $r_{JH} = +0.74$, $r_{HK'} = +0.81$, and $r_{JK'} = +0.71$ for the entire sample, for which the 68.3% confident interval is about 0.1 or less. The coefficient is higher than +0.59 for the radio-quiet sample, and even higher than +0.8 for the radio-loud sample.

Figure 8 shows the z -dependence of r_{JH} , $r_{HK'}$, and $r_{JK'}$. For the radio-quiet sample, all these coefficients at $z < 0.1$ are equally high. While r_{JH} keeps a high value irrespective of z , the coefficients $r_{JK'}$ and $r_{HK'}$ are getting smaller for higher z . This trend may have occurred from an underestimation of the correlation, because of lower statistical accuracy in the high- z sample of smaller size, and because of larger errors in Δm for the high- z sample consisting mainly of faint AGNs. For the radio-loud sample, all the coefficients keep a high value irrespective of z and their accuracy becomes higher for higher z , in sharp contrast with the radio-quiet sample.

The equivalence of r_{JH} , $r_{HK'}$, and $r_{JK'}$ was tested against the estimated true value of coefficient r_{true} . Table 5 tabulates the estimation of r_{true} together with P which represents the reliability of rejecting the hypothesis that r_{JH} , $r_{HK'}$, and $r_{JK'}$ are equivalent to each other. For the radio-quiet sample, their equivalence at $z = 0.1 - 0.3$ is significantly rejected, while not definitely so at higher z . For the radio-loud sample, the equivalence at $z > 0.3$ is rejected with negligible reliability, in other words, it is very probable that r_{JH} , $r_{HK'}$, and $r_{JK'}$ are the same at $z > 0.3$.

It is important to note that r_{JH} , $r_{HK'}$, and $r_{JK'}$ for the radio-quiet sample are equally high at $z < 0.1$, and $r_{HK'}$ is higher than r_{JH} and $r_{JK'}$ at $z = 0.1 - 0.3$. In dust reverberation

model, the NIR flux of AGNs is mainly emitted from hot dust which is heated up to the evaporation temperature $T_{\text{evap}} \approx 1500\text{K}$ (e.g., Kobayashi et al. 1993). The equivalence of r_{JH} , $r_{HK'}$, and $r_{JK'}$ at $z < 0.1$ can be explained by the black body radiation with constant $T_{\text{evap}} \approx 1500\text{K}$ dominating on the longer-wavelength region of the $1\mu\text{m}$ minimum seen in the rest-frame SED of AGNs and quasars. On the other hand, the main variable component dominating on the shorter-wavelength region of the $1\mu\text{m}$ minimum is considered to be a power-law component, and its variability is not necessarily synchronized with the NIR variability. Figure 9 shows this non-synchronization between UV/optical and NIR variabilities on either sides of $1\mu\text{m}$ in rest frame. Thereby, at $z = 0.1 - 0.3$, the correlation of variabilities between the J band and longer wavelengths becomes weak, because the $1\mu\text{m}$ minimum in the rest frame moves to the J band and the power-law variable component affects the flux there. At $z > 0.3$, the $1\mu\text{m}$ minimum moves in between the H and K' band. In such case, r_{JH} is kept high, determined mainly by the the power-law variable component, while $r_{HK'}$ and $r_{JK'}$ become low, determined by both the power-law and black-body components.

For the radio-loud sample, however, the observed trends of r_{JH} , $r_{HK'}$, and $r_{JK'}$ are very different from those for the radio-quiet sample and may be explained by a mechanism of variability other than dust reverberation.

3.4. The time scale of AGN variability

In this section we consider the relation between the time scale and other parameters that characterize the variability of AGNs. For pedagogical purpose, we introduce two representative functions to be fitted to our NIR data:

$$\Delta m(A, p) = A(\Delta t_{\text{rest}})^p \quad , \quad (4)$$

and

$$\Delta m(B, \tau) = B(1 - \exp(-\Delta t_{\text{rest}}/\tau)) \quad . \quad (5)$$

These functions correspond to a divergent increase of variability and an asymptotic increase with increasing Δt_{rest} , respectively.

Tables 6a and 6b tabulate the fitted values of the parameters and their 95% and 99% confidence intervals, applied to the AGNs in the entire sample as well as the radio-quiet and radio-loud samples. The curves with such fitted values are shown in Fig. 10. We note that p and τ are searched for in their positive values to avoid division by 0 at $\Delta t_{\text{rest}} = 0$ in equations 4 and 5. If their fitted values or the lower limits of their confidence intervals became negative, they were given the value of zero.

All the fitted curves are accepted independent of how the data are divided into subgroups. Thus, it is difficult to prefer the function in equation 4 to the other in equation 5. However, it is generally suggested from Tables 6a and 6b that p and τ for the radio-loud sample are smaller than those for the radio-quiet sample, which indicates that the time scale of NIR variability of radio-loud AGNs is shorter than that for the radio-quiet AGNs.

Figure 11 shows the fitted values of p and τ in comparison with those obtained by Cristiani et al. (1996) from the optical variability data in the literature. The vertical errorbar is for the 68.3% confidence interval, and the horizontal errorbar for the covered range of wavelengths. It is interesting to see that the time scale of optical variability by Cristiani et al. (1996) agrees, within the range of uncertainties, with the time scale of NIR variability for the radio-quiet sample. On the contrary, this is not the case for the radio-loud sample, where the time scale of optical variability is significantly longer than the time scale of NIR variability.

From the viewpoint of dust reverberation, it is natural that the NIR variability occurs on a rather elongated time scale, because the UV/optical variability is re-emitted in the

NIR from a more extended region of dust producing a spread of arrival times. Consequently, whether the NIR variability occurs as fast as or faster than the UV/optical variability gives a clue which limits or rejects a mechanism of variability based upon the dust reverberation model. In this regard, it is difficult to explain by the dust reverberation model how the NIR variability of the radio-loud AGNs occurs faster than the optical variability, as seen from the comparison in Fig. 11.

3.5. The relation between near infrared variability and radio activity

We have highlighted the difference of NIR variability between the radio-quiet and radio-loud AGNs. Obtained features for these respective samples are summarized as follows:

- (1) The amplitude of ensemble NIR variability Δm in the radio-quiet sample is smaller than in the radio-loud sample.
- (2) The wavelength-dependence of Δm in the NIR region is not found in both the radio-quiet and radio-loud samples.
- (3) No correlation is found between Δm and M_B in the radio-quiet sample, but a negative correlation is suggested if corrected for the effect of possible contamination of a host galaxy component. On the other hand, a positive correlation is found between Δm and M_B in the radio-loud sample.
- (4) The correlation coefficient r_{HK} between the H and K variabilities at $z = 0.1 - 0.3$ is significantly higher than r_{JH} and $r_{JK'}$ in the radio-quiet sample. On the other hand, the coefficients r_{JH} , $r_{JK'}$ and $r_{HK'}$ at $z > 0.3$ have a high value of $0.9 - 0.95$ in the radio-loud sample.

(5) The time scale of NIR variability in the radio-quiet sample is longer than in the radio-loud sample.

The features of 2, 3, and 4 for the radio-quiet AGNs are consistent with those expected from a mechanism of variability by dust reverberation. Furthermore, the feature of 5 for the radio-quiet AGNs, if combined with the time scale of optical variability by Cristiani et al. (1996), is also consistent with dust reverberation.

However, the features of 2 to 5 for the radio-loud AGNs are not explained consistently by dust reverberation. A non-thermal variable component, as a substitute of thermal radiation from hot dust, is worth considering. For example, Sanders et al. (1989) proposed such a non-thermal component which would vary more strongly and faster in the compact region than the thermal radiation from an extended hot dust torus.

We proceed with the working hypothesis such that dust reverberation is responsible for the emission and variability of radio-quiet AGNs, while a non-thermal variable component is responsible for the emission and variability of radio-loud AGNs. In the next subsections, we check the plausibility of this hypothesis using additional data from the literature.

3.5.1. The radio strength of the dust reverberation sample

It is known that the time delay of NIR variability lagged behind the the UV/optical variability is a key prediction of the dust reverberation model. Therefore, measurements of UV/optical and NIR light curves, based on multi-wavelength monitoring observations of AGNs, immediately reject or justify the application of the dust reverberation model to individual AGNs.

The AGNs with measured time delay, to which the dust reverberation model is successfully applied, are taken from the literature, and their data of z , M_B , and

$f_\nu(6\text{cm})/f_\nu(V)$ are summarized in Table 7. It is evident that these AGNs are classified as radio-quiet with $f_\nu(6\text{cm})/f_\nu(V) < 10$. The sample of these AGNs is heterogeneous and is far from complete. It is possible that the sample is biased in favor of nearby and/or radio-quiet AGNs.

The first systematic monitoring observations of many Seyfert 1 AGNs and quasars in the V and K bands were performed by Nelson (1996a). Table 8 shows the statistics based on Nelson’s sample consisting of 51 program AGNs. The first row represents the numbers of radio-quiet and radio-loud AGNs in his entire sample of 51 AGNs, the second row for the subsample of 33 AGNs which were found to vary in both the V and K bands, and the third row for the subsample of 6 AGNs for which the time delay of the K -band variability relative to the V -band variability were measured.

We see that the AGNs with measured time delay, which are best explained by the simple dust reverberation model, are always classified as radio-quiet. In other words, radio-quiet AGNs are potential targets for multi-wavelength monitoring from which the time delay between the NIR and UV/optical variabilities can certainly be measured.

3.5.2. *The relation between variability and flatness of radio SED*

The large and fast NIR variability of radio-loud AGNs found in this paper is not explained by dust reverberation model. In order to understand what causes such variability, we further classify the radio-loud AGNs with respect to their spectral feature in the radio region, being either flat ($\alpha > -0.5$) or steep ($\alpha < -0.5$), if fitted to a power-law form of $f_\nu \propto \nu^\alpha$ (Sanders et al. 1989).

The values of power index α in our sample were determined using the data of radio fluxes at 6 cm and 11 cm taken from the VV catalog. Figure 12 shows that α is not

correlated with M_B or z . Figure 13 shows that the ensemble variability in the J , H , and K' bands is $\Delta m \approx 0.35 - 0.45$ for the radio-loud and flat-spectrum AGNs, which is systematically higher than $\Delta m \approx 0.2$ for the radio-loud and steep-spectrum AGNs. It is therefore the flat component that actually brings about the large and fast NIR variability.

The radio spectral index, α , is known to be well correlated with the radio-loud AGN morphology; while the steep spectrum is associated with extended lobe-dominant sources, the flat spectrum is associated with core-dominant variable sources such as OVVs, highly polarized QSOs, and BL lacs. Thereby, it is reasonable to conclude that a non-thermal variable component, as exemplified by non-thermal emissions from such objects (e.g., Robson et al. 1993; Bloom et al. 1994), is responsible for occurrence of features of the NIR variability found for the radio-loud AGNs in this paper.

4. Summary

We presented comprehensive study of NIR variability of 226 AGNs based on multiple observations in the J , H , and K' bands. Our sample consists mainly of Seyfert 1 AGNs and QSOs. About a quarter of objects in each category are radio loud. The AGNs in the entire sample have redshifts spanning a range from $z = 0$ to 1, and the absolute B -magnitudes from $M_B = -29$ to -18 .

Based on the method of differential photometry, we find that the ensemble NIR variability for the entire sample of AGNs is typically $\Delta m \approx 0.2$ mag. When the sample is divided by radio strength, the variability for the radio-quiet sample is systematically smaller than that for the radio-loud sample. No clear wavelength-dependence of Δm in the NIR region is found for either the radio-quiet or radio-loud sample, in sharp contrast with the UV/optical result in the literature.

We examined the dependence of Δm on various quantities such as radio strength, M_B , and z , with special attention as to whether their ensemble variability would support or reject the simple-minded dust reverberation model for AGNs.

The radio-quiet AGNs show no significant correlation between Δm and M_B , although negative correlation is suggested if corrected for the effect of possible contamination by a host galaxy component. On the other hand, the radio-loud AGNs show a positive correlation between Δm and M_B .

The radio-quiet AGNs give a significantly higher correlation coefficient r_{HK} between the H and K variabilities at $z = 0.1 - 0.3$, when compared to r_{JH} and $r_{JK'}$. On the other hand, the radio-loud AGNs give a high value of $0.9 - 0.95$ to all the coefficients r_{JH} , $r_{JK'}$ and $r_{HK'}$ at $z > 0.3$.

Time development of ensemble variability is examined using heuristic functions. The time scale of NIR variability for the radio-quiet AGNs in this paper is not shorter than the time scale of UV/optical variability given in the literature. However, the time scale of NIR variability of the radio-loud AGNs is significantly shorter than the time scale of their UV/optical variability.

All the features of NIR variability for the radio-quiet AGNs are consistent with those expected from the dust reverberation model. However, it is difficult for this simple-minded model to explain the features of the radio-loud AGNs, and a non-thermal variable component is suggested as a viable candidate for causing the large and fast NIR variability of the radio-loud AGNs.

We are grateful to H. Okuda, M. Narita and other staff of the infrared astronomy group of the Institute of Space and Astronautical Science (ISAS) for their support in using their 1.3m telescope. We thank the staff of the Advanced Technology Center of the National

Astronomical Observatory of Japan (NAOJ) for their new coating of the mirror of the 1.3m telescope at the ISAS. Gratitude is also extended to the Computer Data Analysis Center of the NAOJ. This work has made use of the NASA/IPAC Extra Galactic Database (NED), and has been supported partly by the Grand-in-Aid (07CE2002, 10304014) of the Ministry of Education, Science, Culture, and Sports of Japan and by the Torey Science Foundation.

A. estimation of the ensemble variability

This section describes how we estimate variability and its error in this work using the data for which the sample number and accuracy are both limited. The data obtained in this work are given in the format of $(\Delta m_1, \sigma_1), (\Delta m_2, \sigma_2) \dots (\Delta m_N, \sigma_N)$ for the sample of $\text{AGN}_1, \text{AGN}_2 \dots \text{AGN}_N$. Here, Δm_i and σ_i represent the variability and its error of the i -th object. Hereafter, the real variability of the i -th object is described as v_i , and the difference between v_i and Δm_i is given by e_i . Then, e_i can be regarded as a random variable described by the normal distribution having zero average and the standard deviation σ_i , that is,

$$\Delta m_i = v_i + e_i, \quad \langle e_i \rangle = 0, \quad \langle e_i^2 \rangle = \sigma_i^2, \quad (\text{A1})$$

where $\langle \rangle$ represents the expectation. The real variability of the i -th object v_i is assumed to be a random variable that follows the normal distribution with zero average and the standard deviation v_0 independent of i .

In the ideal case where the data have zero error and the sample size is infinite, the dispersion of variability is given by

$$\lim_{N \rightarrow \infty} \left[\frac{\sum_i^N v_i^2}{N} \right] \quad (\text{A2})$$

Hereafter, the aim is to estimate the value of equation A2 and the error from the existing data. Consider

$$v_i^2 = \Delta m_i^2 - 2v_i e_i - e_i^2. \quad (\text{A3})$$

Then, the expectation of the second term in the right-hand side vanishes because v_i and e_i are independent of each other. Therefore, the expectation of v_i^2 becomes

$$\langle v_i^2 \rangle = \Delta m_i^2 - \sigma_i^2. \quad (\text{A4})$$

Substitution of the observed data into equation A2 gives

$$\lim_{N \rightarrow \infty} \left[\frac{\sum_i^N v_i^2}{N} \right] \sim \frac{\sum_i^N v_i^2}{N} \sim \frac{\sum_i^N \Delta m_i^2 - \sum_i^N \sigma_i^2}{N} \equiv \overline{v_0^2}, \quad (\text{A5})$$

where the first \sim stems from the finite sample number and the second \sim stems from the error of the data. The overline of $\overline{v_0^2}$ indicates that the value is the expectation based on the existing data.

The error of equation A5 is estimated as follows: First, we focus on the error caused by the deviation of the ideal expectation from that of the actual data with finite sample number. It should be noticed that $\sum_i^N (v_i/v_0)^2$ is the random variable described by the χ^2 distribution with N degrees of freedom. Since v_i/v_0 ($i = 1, 2, \dots, N$) is a random variable that follows the normal distribution with zero average and the standard deviation of unity, the expectation $\sum_i^N (v_i/v_0)^2$ is equal to N with the dispersion of $2N$. Therefore, the error of equation A5 arising from the finite sample number is estimated as $\pm \sqrt{2v_0^4/N}$.

We next focus on the error caused by the deviation of the ideal expectation from that of the actual data with non-zero error. Assuming that v_i and e_i are independent of each other, the difference between v_i^2 and $\langle v_i^2 \rangle$ is calculated as

$$\begin{aligned} \langle (v_i^2 - \langle v_i^2 \rangle)^2 \rangle &= \langle (\Delta m_i^2 - 2e_i v_i - e_i^2 - \Delta m_i^2 + \sigma_i^2)^2 \rangle \\ &= \langle 4e_i^2 v_i^2 + e_i^4 + \sigma_i^4 + 4e_i^3 v_i - 4e_i v_i \sigma_i^2 - 2e_i^2 \sigma_i^2 \rangle \\ &= 4\sigma_i^2 \langle v_i^2 \rangle + \langle e_i^4 \rangle - \sigma_i^4, \end{aligned} \quad (\text{A6})$$

where equation A1 is used. Using equation A4 and $\langle e_i^4 \rangle = 3\sigma_i^4$, equation A6 furthermore reduces to

$$\langle (v_i^2 - \langle v_i^2 \rangle)^2 \rangle = 4\sigma_i^2 \langle v_i^2 \rangle + 2\sigma_i^4$$

$$= 4\sigma_i^2 \Delta m_i^2 - 2\sigma_i^4. \quad (\text{A7})$$

Therefore, the error of equation A5 arising from the non-zero error of the variability data is estimated as $\pm \sqrt{\sum_i^N (4\Delta m_i^2 \sigma_i^2 - 2\sigma_i^4)/N^2}$. Using equation A5 and the above error estimates, the expectation value of v_0^2 and its error are estimated as

$$\begin{aligned} \overline{v_0^2} &= \frac{\sum_i^N \Delta m_i^2 - \sum_i^N \sigma_i^2}{N} \pm \sqrt{\frac{2v_0^4}{N} + \frac{\sum_i^N (4\Delta m_i^2 \sigma_i^2 - 2\sigma_i^4)}{N^2}} \\ &\sim \frac{\sum_i^N \Delta m_i^2 - \sum_i^N \sigma_i^2}{N} \pm \sqrt{\frac{2(\sum_i^N \Delta m_i^2 - \sum_i^N \sigma_i^2)^2}{N^3} + \frac{\sum_i^N (4\Delta m_i^2 \sigma_i^2 - 2\sigma_i^4)}{N^2}}. \end{aligned} \quad (\text{A8})$$

Finally, using the usual error propagation, the expectation value of v_0 and its error are estimated as

$$\begin{aligned} \overline{v_0} &= \sqrt{\frac{\sum_i^N \Delta m_i^2 - \sum_i^N \sigma_i^2}{N}} \\ &\pm \frac{1}{2} \left[\frac{\sum_i^N \Delta m_i^2 - \sum_i^N \sigma_i^2}{N} \right]^{-1/2} \sqrt{\frac{2(\sum_i^N \Delta m_i^2 - \sum_i^N \sigma_i^2)^2}{N^3} + \frac{\sum_i^N (4\Delta m_i^2 \sigma_i^2 - 2\sigma_i^4)}{N^2}}. \end{aligned} \quad (\text{A9})$$

REFERENCES

- Baribaud, T., Alloin, D., Glass, I. and Pelat, D. 1992, *A&A*, 256, 375
- Barvanis,R., 1992, *ApJ*, 400, 502
- Bloom,S.D., Marscher,A.P., Gear,.K., Terasranta,H., Valtaoja,E., Aller,H.D. and Aller,M.F.
1994, *AJ*, 108, 398
- Cimatti, A., Zamorani, G., and Marano, B., 1993, *MNRAS*, 263, 236
- Clavel, J., Wamsteker, W., and Glass, I. S. 1989, *ApJ*, 337, 236
- Cristiani, S., Trentini, S., La Franca, F., Aretxaga, I., Andreani,P., Vio, R., Gemmo, A.
1996, *A&A*, 306, 395
- Cristiani, S., Trentini, S., La Franca, F., and Andreani, P. 1997, *A&A*, 321, 123
- Cristiani, S., Vio, R., and Andreani, P. 1990, *MNRAS*, 245, 493
- Di Clemente,A., Giallongo,E., Natali,G., Trevese,D. and Vagnetti,F. 1996, *ApJ*, 463, 466
- Glass, I. S. 1992, *MNRAS*, 256, 23
- Hook, I. M., McMahon, R. G., Boyle, B. J., and Irwin, M. J. 1994, *MNRAS*, 268, 305
- Kobayashi, Y., Yoshii, Y., Peterson, Bruce A., Miyazaki, S., Aoki, T., Minezaki, T.,
Kawara, K., Enya, K., Okada, N., Suganuma, M., Greene, B., O'Brien, M., Randall,
and Lawrence K. 1998a, *Proc. SPIE Vol. 3352*, p. 120-128, *Advanced Technology
Optical/IR Telescopes VI*, Larry M. Stepp, Ed.
- Kobayashi, Y., Yoshii, Y., Peterson, Bruce A., Minezaki, T., Enya, K., Suganuma, M.,
and Yamamuro, T. 1998b, *Proc. SPIE Vol. 3354*, p. 769-776, *Infrared Astronomical
Instrumentation*, Albert M.Fowler, Ed.
- Kobayashi, Y., Fang, G., Minezaki, T., Waseda, K., Nakamura, K., and Sato, S. 1994, *Proc.
SPIE Vol. 2198*, p. 603-613, *Instrumentation in Astronomy VIII*, David L. Crawford,
Eric R. Craine, Eds.

- Kobayashi, Y., Sato, S., Yamashita, T., Shiba, H., and Takami, H. 1993, *ApJ*, 404, 94
- Kotilainen, J. K., and Ward, M. J. 1994, *MNRAS*, 266, 953
- Nelson, B. O., 1996a, Doctor thesis
- Nelson, B. O. 1996b, *ApJ*, 465, L87
- Neugebauer, G., Soifer, B. T., Matthews, K., and Elias, J. H. 1989, *AJ*, 97, 957
- Oknyanskii, V. L. 1993, *Astron. Lett.*, 19, 416
- Robson, E. I., Litchfield, S. J., Gear, W. K., Hughes, D. H., Sandell, G., Courvoisier, T. J.-L., Paltani, S., Valtaoja, E., Terasranta, H., Tornikoski, M., and Steppe, H. & Wright, M. C. H. 1993, *MNRAS*, 262, 249
- Sanders, D. B., Phinney, E. S., Neugebauer, G., Soifer, B. T., and Matthews, K. 1989, *ApJ*, 347, 29
- Sitko, M. L., Sitko, A. K., Siemiginowska, A. and Szczerba, R. 1993, *ApJ*, 409, 139
- Trevese, D., Kron, R. G., Majewski, S. R., Bershadsky, M. A. and Koo, D. C. 1994, *ApJ*, 433, 494
- Veron-Cetty, M.-P., and Veron, P. ESO Scientific Report, Garching: European Southern Observatory (ESO), 1993, 6th ed.
- Veron-Cetty, M.-P., and Veron, P. ESO Scientific Report, Garching: European Southern Observatory (ESO), 1996, 7th ed.
- Veron-Cetty, M.-P., and Veron, P. 1998, A Catalogue of quasars and active nuclei, Edition: 8th ed., Publisher: Garching: European Southern Observatory (ESO), 1998, Series: ESO Scientific Report Series vol no: 18
- Winkler, H., Glass, I. S., van Wyk, F., Marang, F., Jones, J. H. S., Buckley, D. A. H. and Sekiguchi, K. 1992, *MNRAS*, 257, 659

Winkler, H. 1997, MNRAS, 292, 273

Fig. 1.— The ensemble variability of AGNs in the J , H and K' bands. Shown are the results for all AGNs, and radio-quiet and loud AGNs (*upper panel*), for radio-quiet AGNs divided by Δt_{rest} (*lower left panel*), and for radio-loud AGNs divided by Δt_{rest} (*lower right panel*). Only the data with more than two reference objects and with accuracy higher than 0.1mag are plotted.

Fig. 2.— The ensemble variability of radio-quiet AGNs in the J , H and K' bands. Shown are the results for short- Δt_{rest} AGNs divided by M_B (*upper left panel*) or by z (*lower left panel*), and those for long- Δt_{rest} AGNs divided by M_B (*upper right panel*) or by z (*lower right panel*).

Fig. 3.— The ensemble variability of radio-loud AGNs in the J , H and K' bands. Shown are the results for short- Δt_{rest} AGNs divided by M_B (*upper left panel*) or by z (*lower left panel*), and those for long- Δt_{rest} AGNs divided by M_B (*upper right panel*) or by z (*lower right panel*).

Fig. 4.— The relation among characteristic parameters for radio-quiet AGNs. Shown are Δm , Δt_{rest} , and M_B plotted against z (*left column*), and Δm , Δt_{rest} , and z plotted against M_B (*right column*).

Fig. 5.— The relation among characteristic parameters for radio-loud AGNs. Shown are Δm , Δt_{rest} , and M_B plotted against z (*left column*), the Δm , Δt_{rest} , and z plotted against M_B (*right column*).

Fig. 6.— The relation between variabilities in two NIR bands for radio-quiet AGNs divided by Δt_{rest} .

Fig. 7.— The relation between variabilities in two NIR bands for radio-loud AGNs divided by Δt_{rest} .

Fig. 8.— The coefficient of correlation r_{ij} between AGN variabilities in the λ_i and λ_j bands as a function of redshift z . Shown are the results for radio-quiet AGNs (*upper panel*), and for radio-loud AGNs (*lower panel*).

Fig. 9.— The ensemble variability of AGNs as a function of rest-frame frequency. Results in the NIR are from this paper, and those in the UV/optical are from the literature. Filled small symbols are for 3 month-data (*triangles*, Cimatti et al. 1993; *filled circles*, Trevese et al. 1994; *squares*, De Clemente et al. 1996; *pentagons*, Hook et al. 1994; *hexagons*, Cristiani et al. 1990). The open small symbols are the same as filled ones, but for 2yr-data.

Fig. 10.— The ensemble variability of AGNs as a function of rest-frame time interval between two observations. Shown are the results for all AGNs (*upper panel*) and for radio-quiet and loud AGNs (*lower panel*). The solid and dotted lines represent the best-fit curves of $\Delta m(A, p) = A(\Delta t_{\text{rest}})^p$ and $\Delta m(B, \tau) = B(1 - \exp(-\Delta t_{\text{rest}}/\tau))$, respectively.

Fig. 11.— The wavelength-dependence of fitted parameters to the ensemble variability of AGNs, such as the power index p in $\Delta m(A, p) = A(\Delta t_{\text{rest}})^p$ (*Upper panel*), and the timescale τ in $\Delta m(B, \tau) = B(1 - \exp(-\Delta t_{\text{rest}}/\tau))$ (*Lower panel*). The vertical errorbars represent the 68.3% confidence interval, and horizontal errorbars represent the range of wavelength coverage in the analysis. Results in the NIR are from this paper, and those in the optical are from Cristiani et al. (1996).

Fig. 12.— The distribution of radio-loud AGNs in the α versus M_B diagram (*upper panel*) and in the α versus z diagram (*lower panel*). The boundary between the steep and flat spectra is placed at $\alpha = -0.5$. Open and filled circles correspond to short- and long- Δt_{rest} samples, respectively.

Fig. 13.— The ensemble variability of radio-loud AGNs in the J , H and K' bands. Shown are the results for those with flat and steep radio spectra.

Figure 1

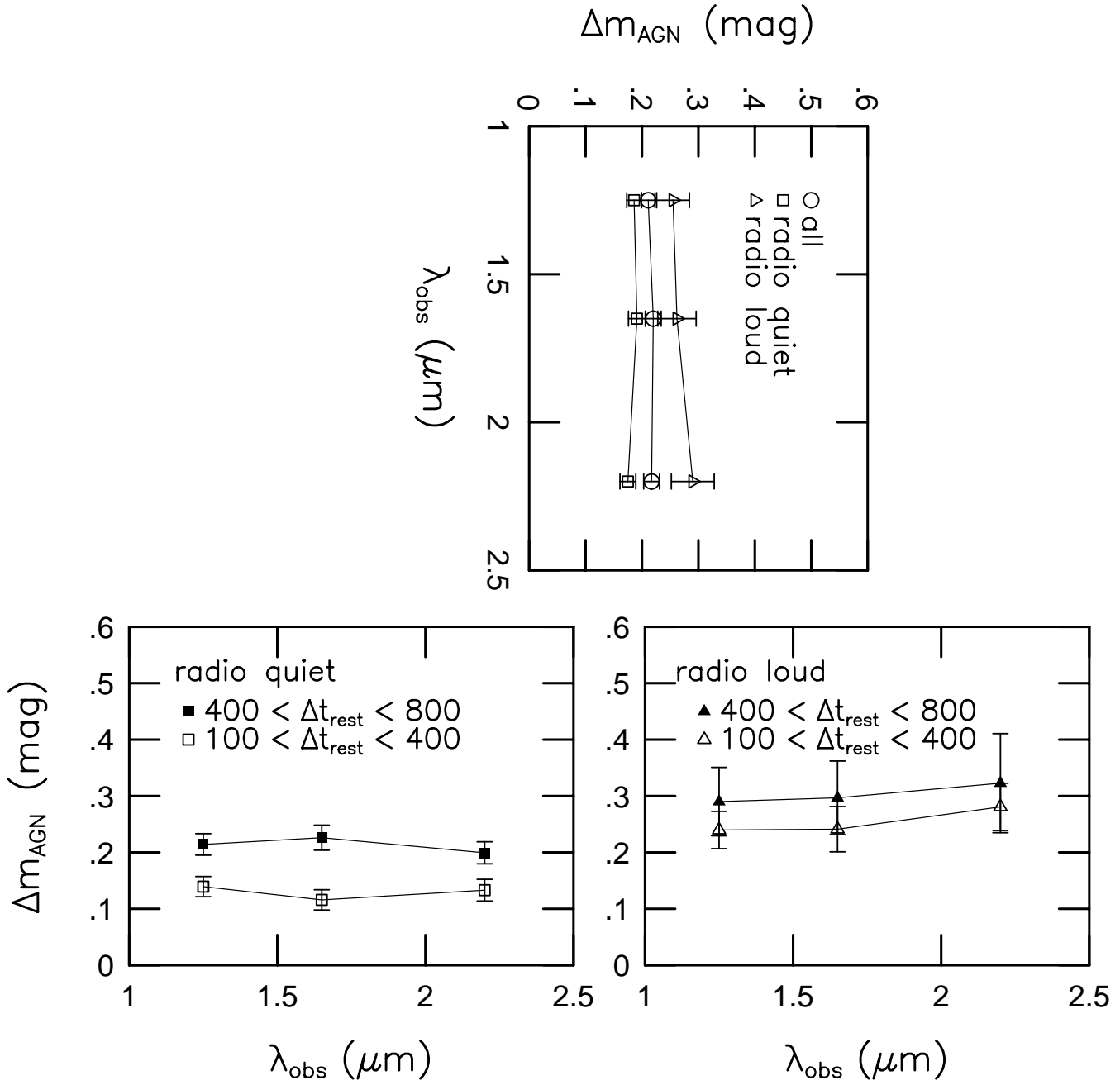


Figure 2

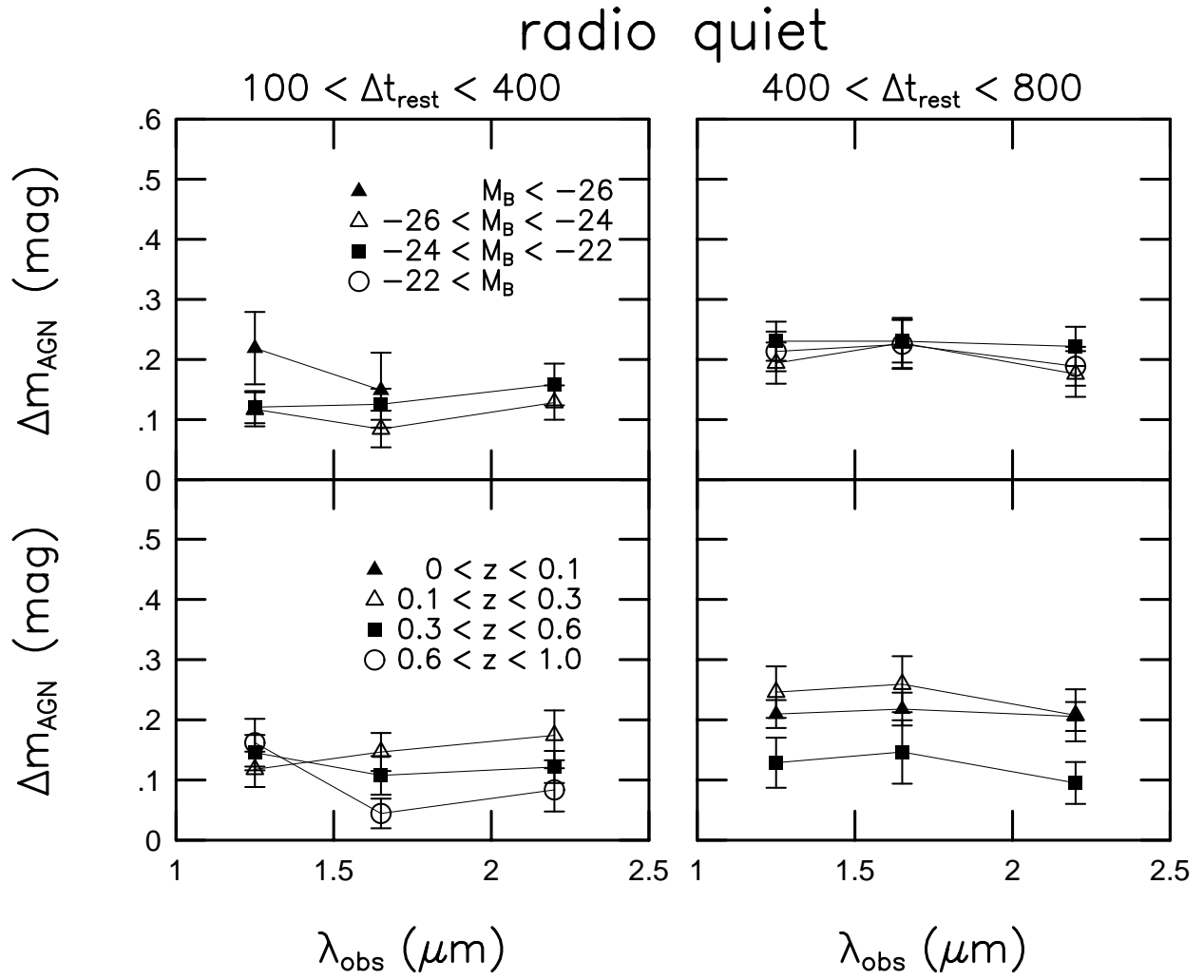


Figure 3

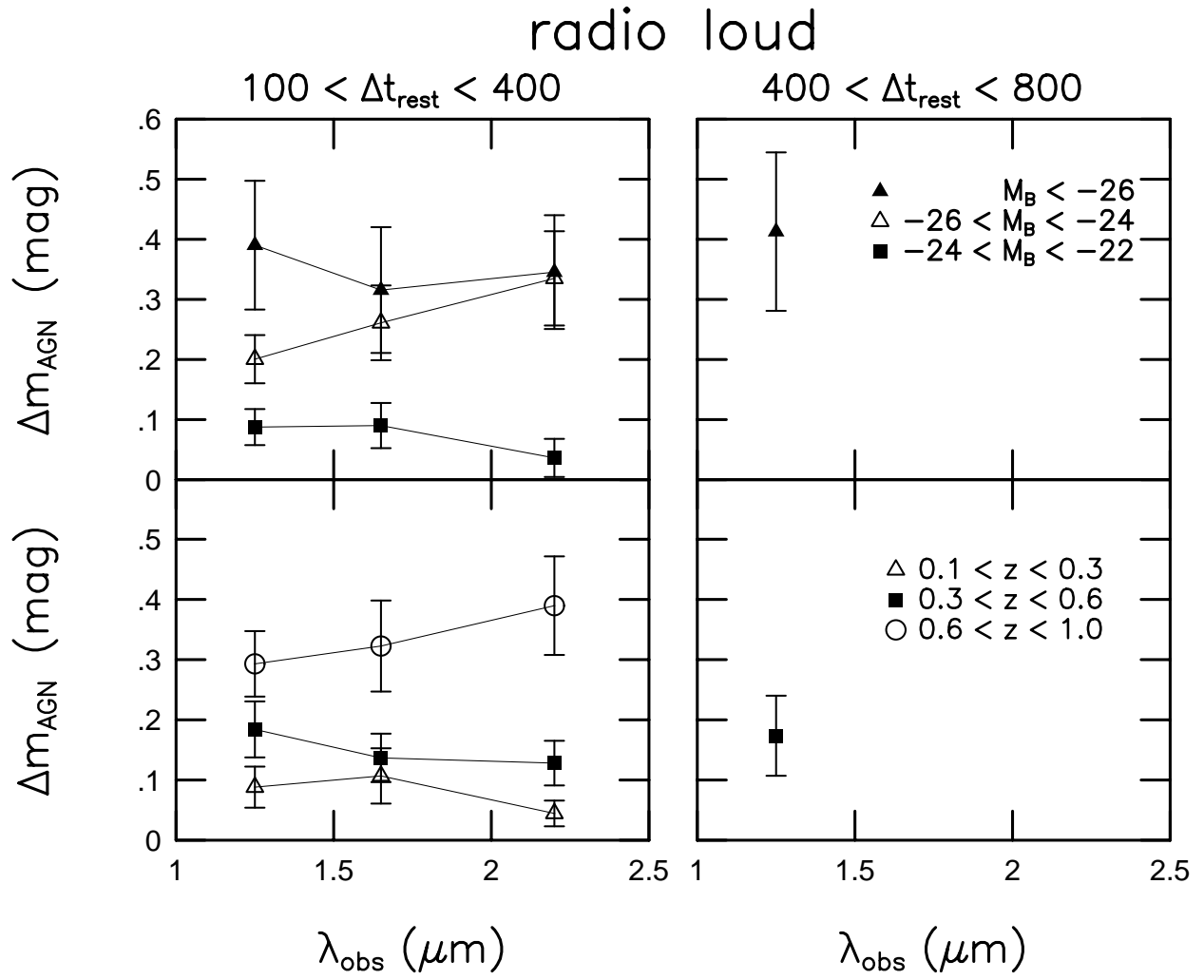


Figure 4

radio quiet

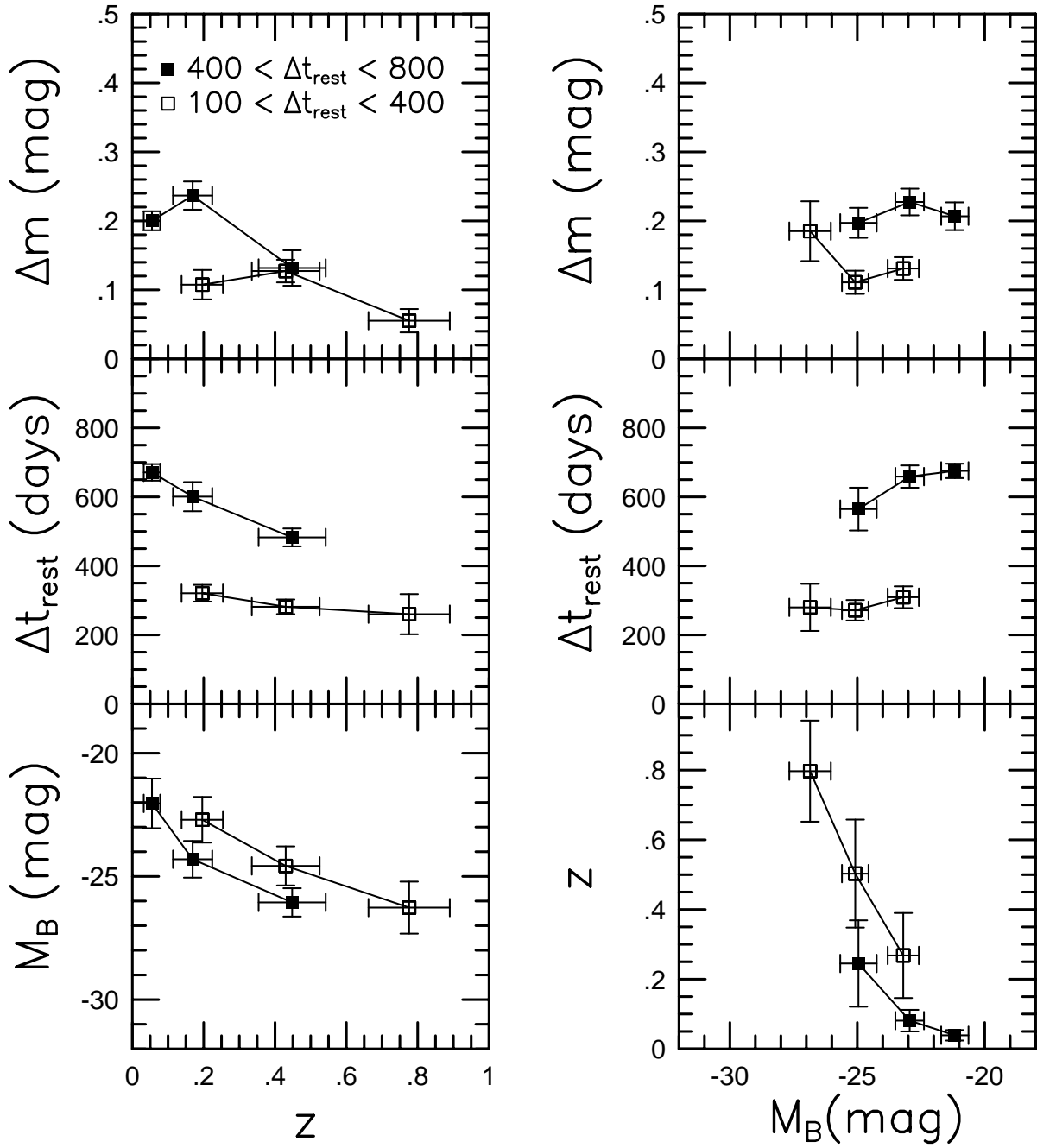


Figure 5

radio loud

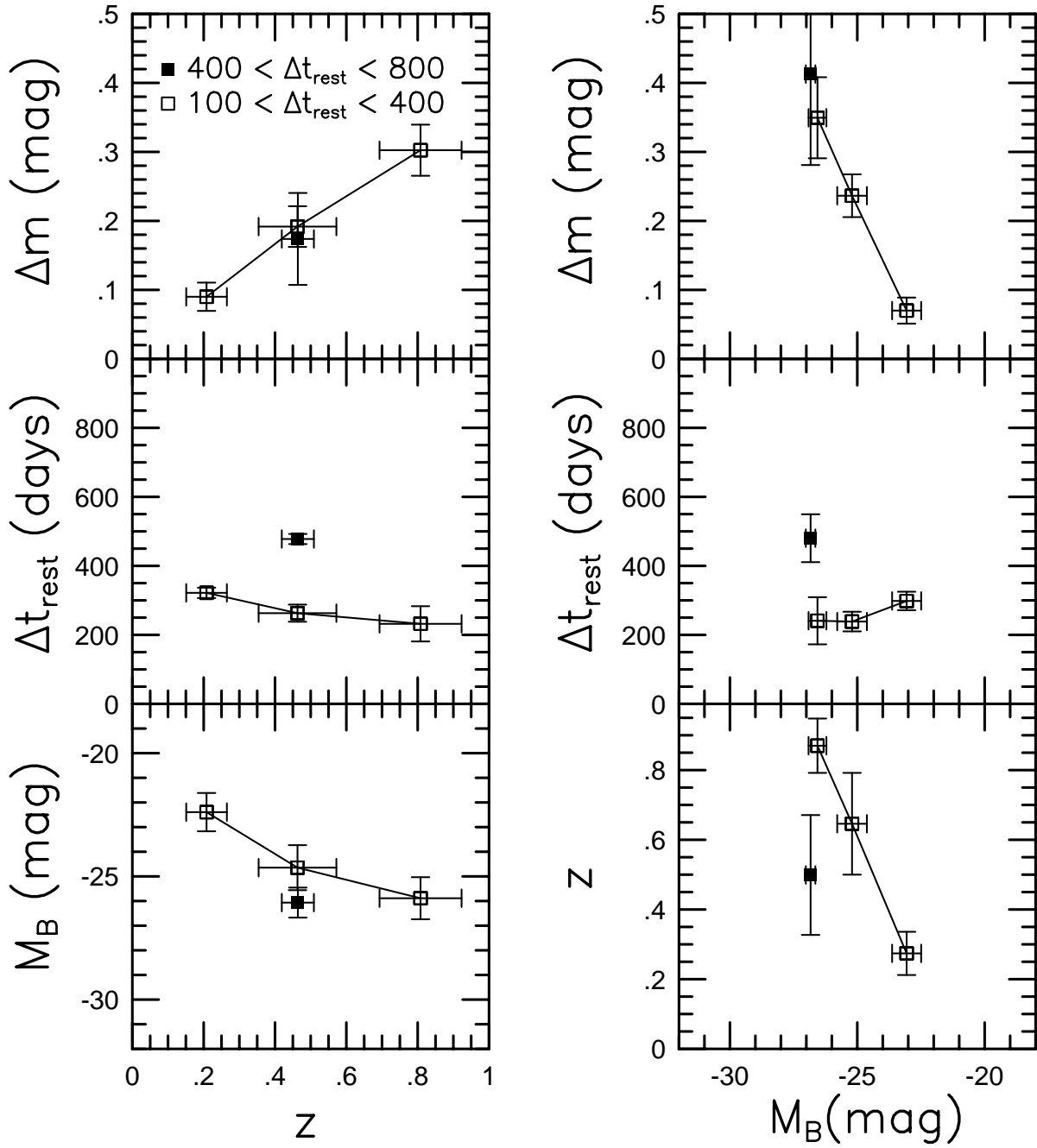


Figure 6

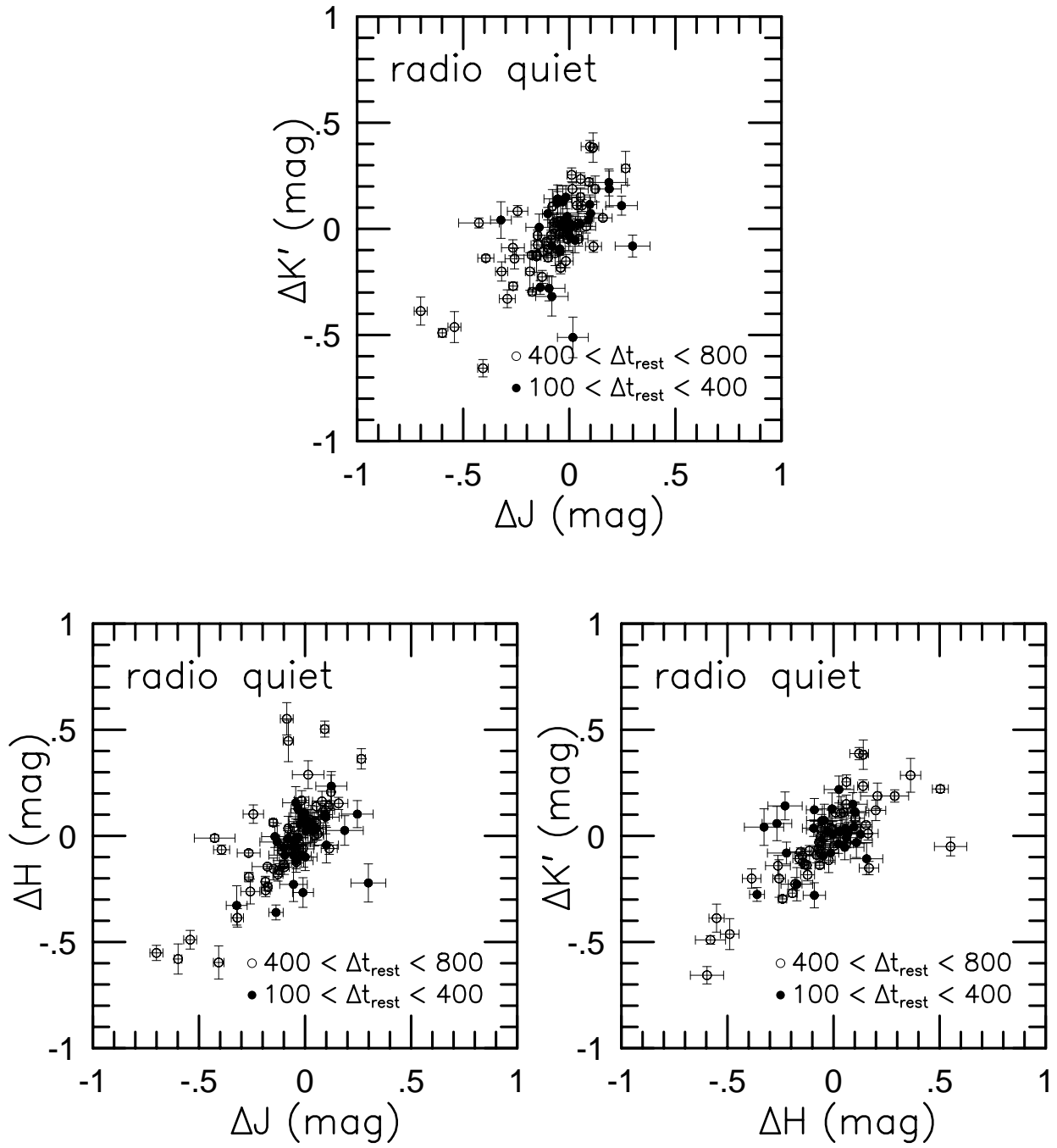


Figure 7

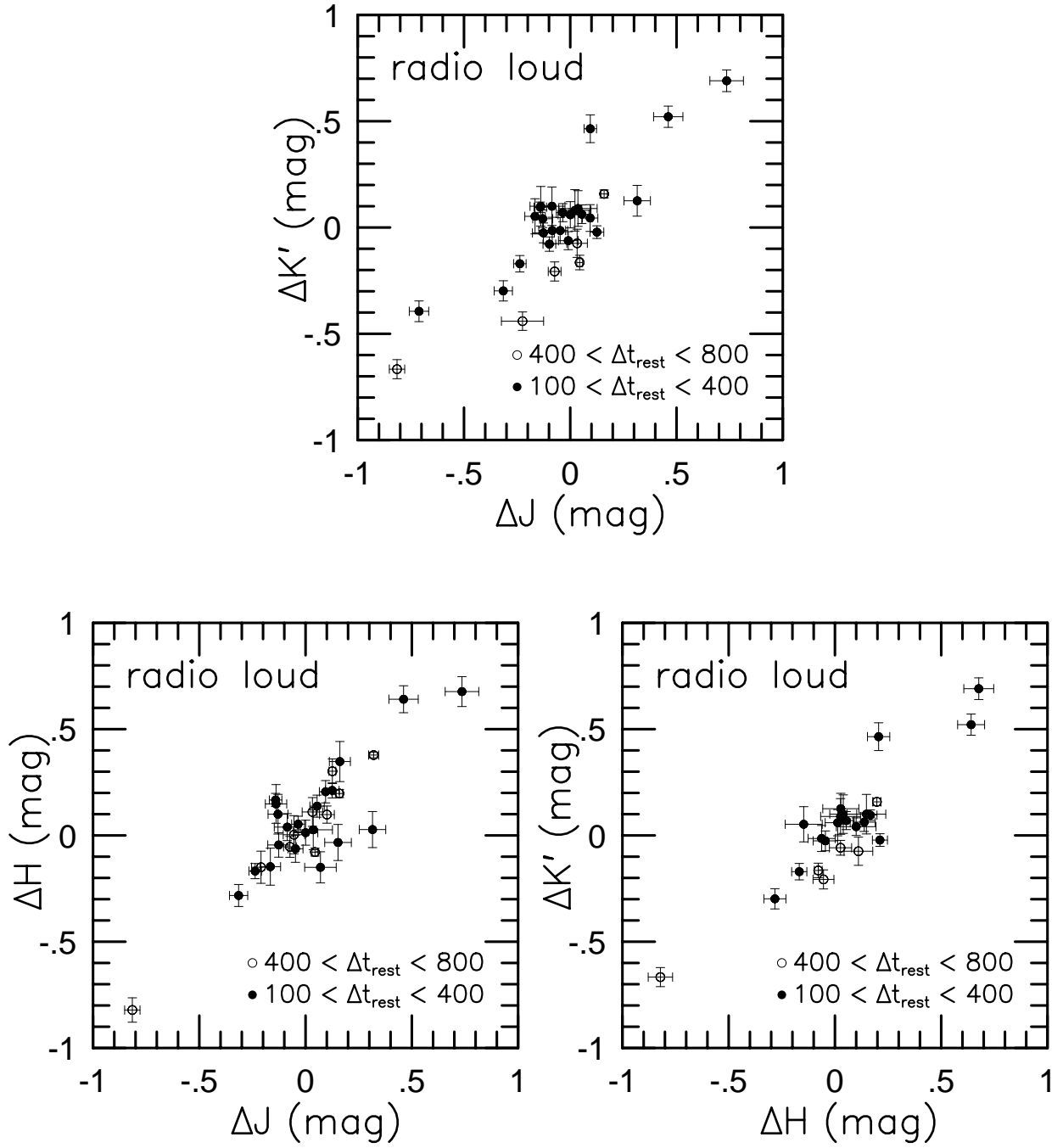


Figure 8

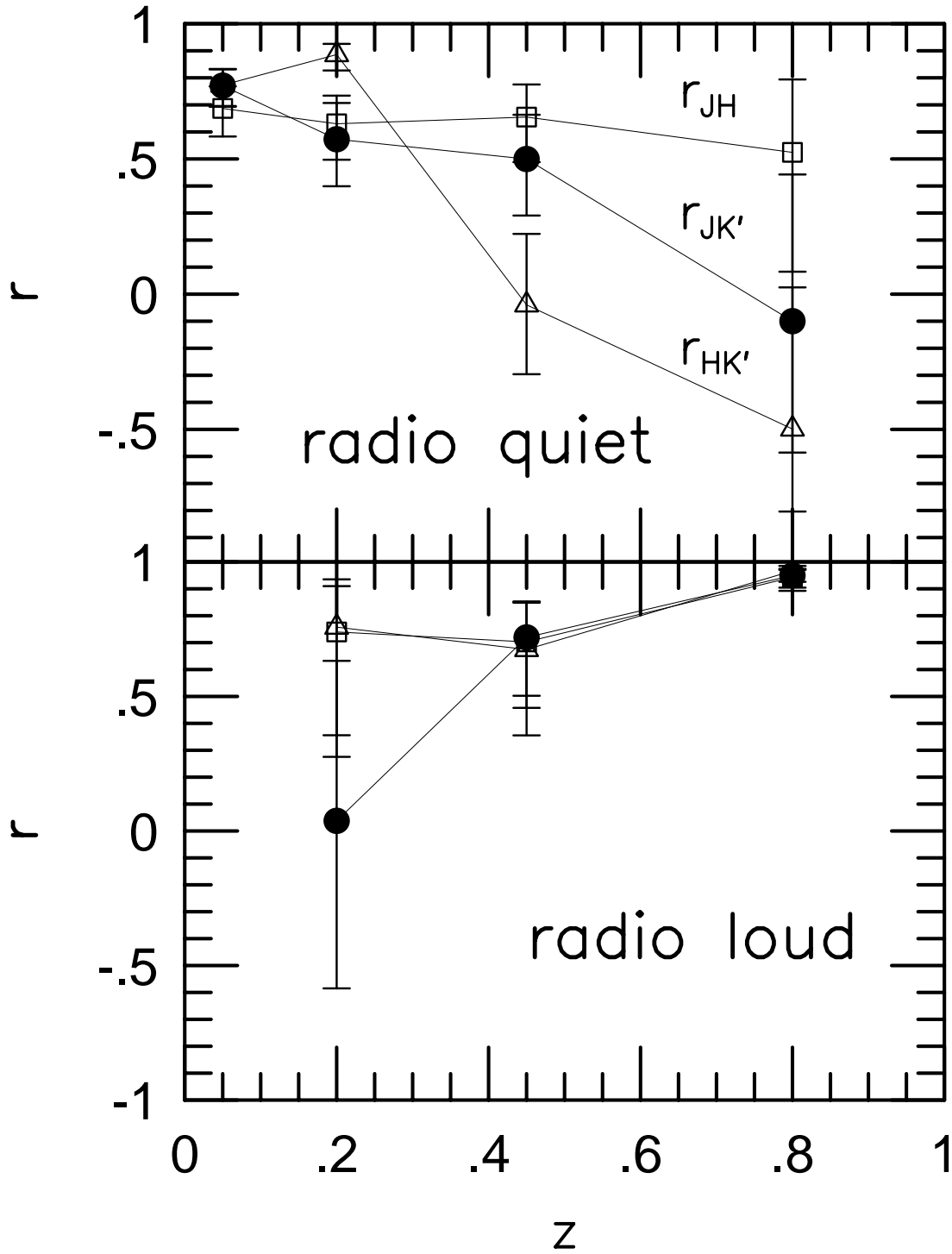


Figure 9

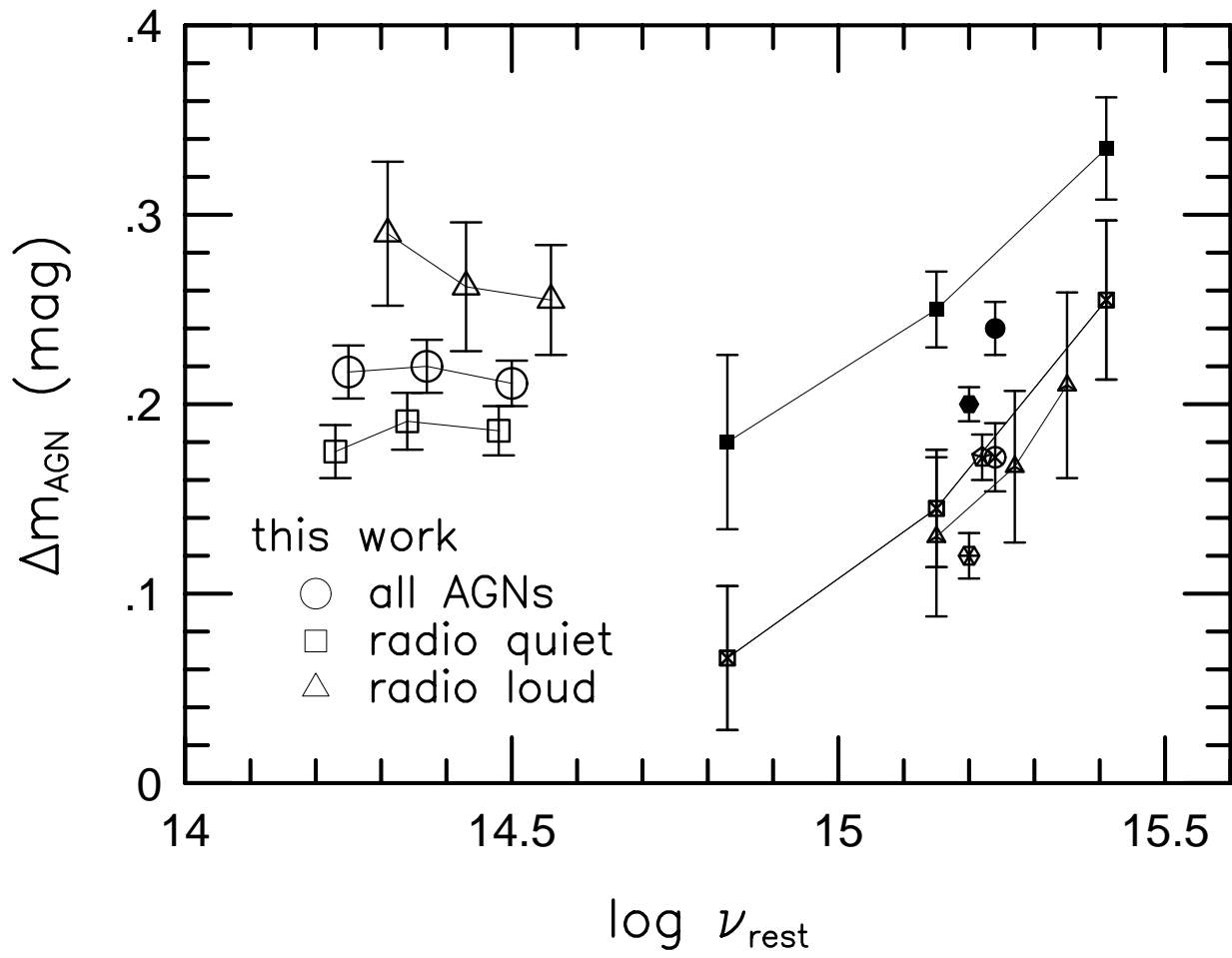


Figure 10

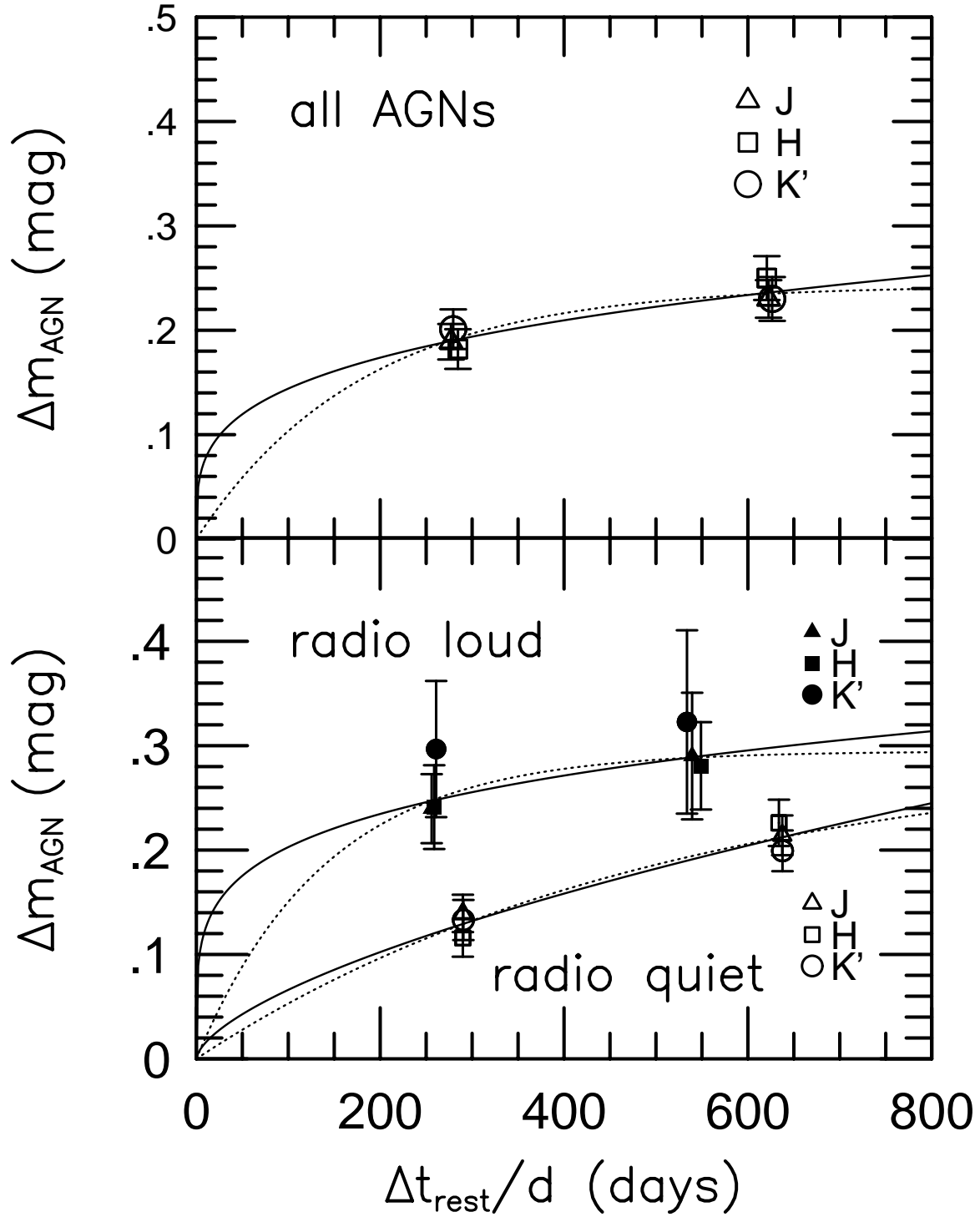


Figure 11

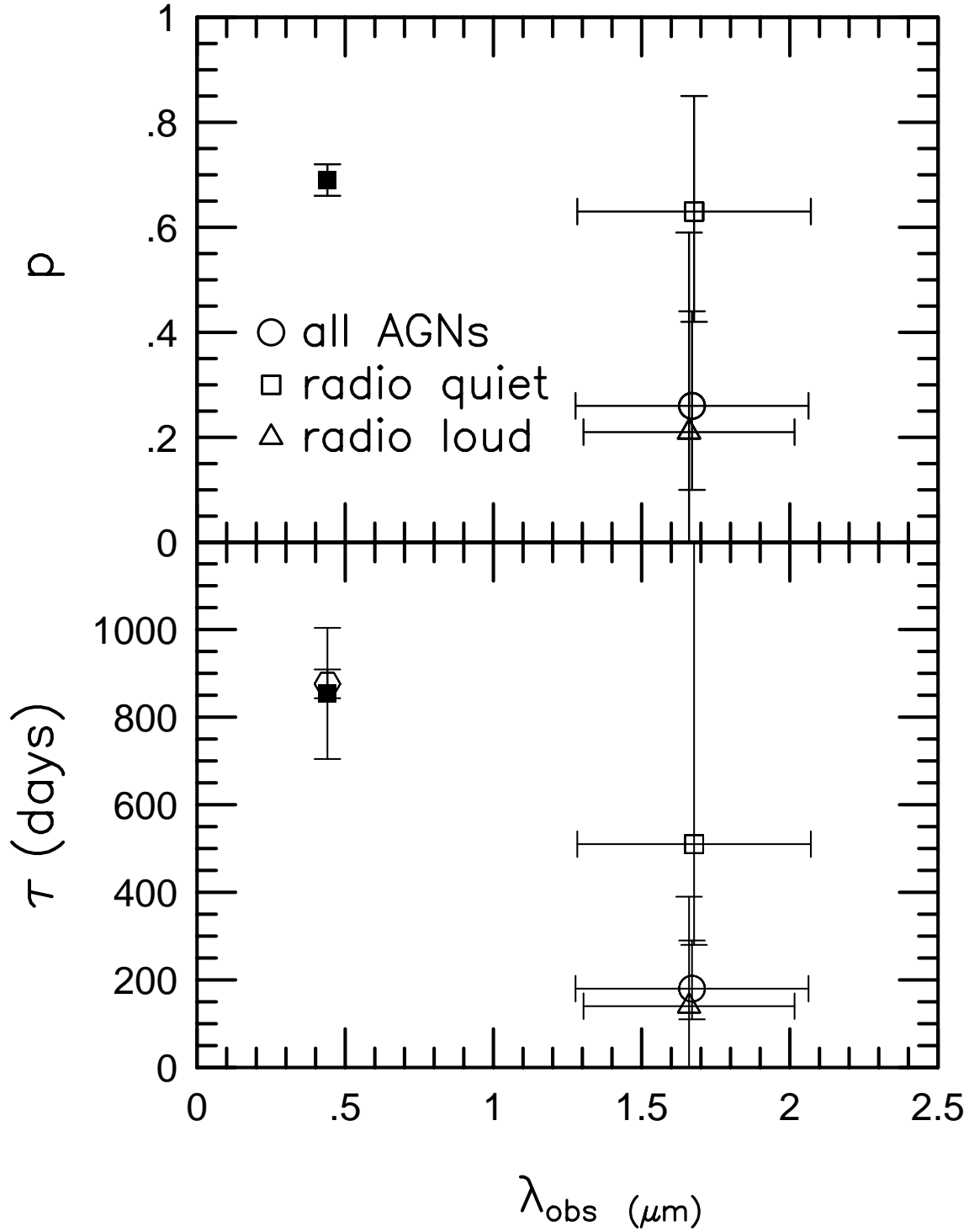


Figure 12

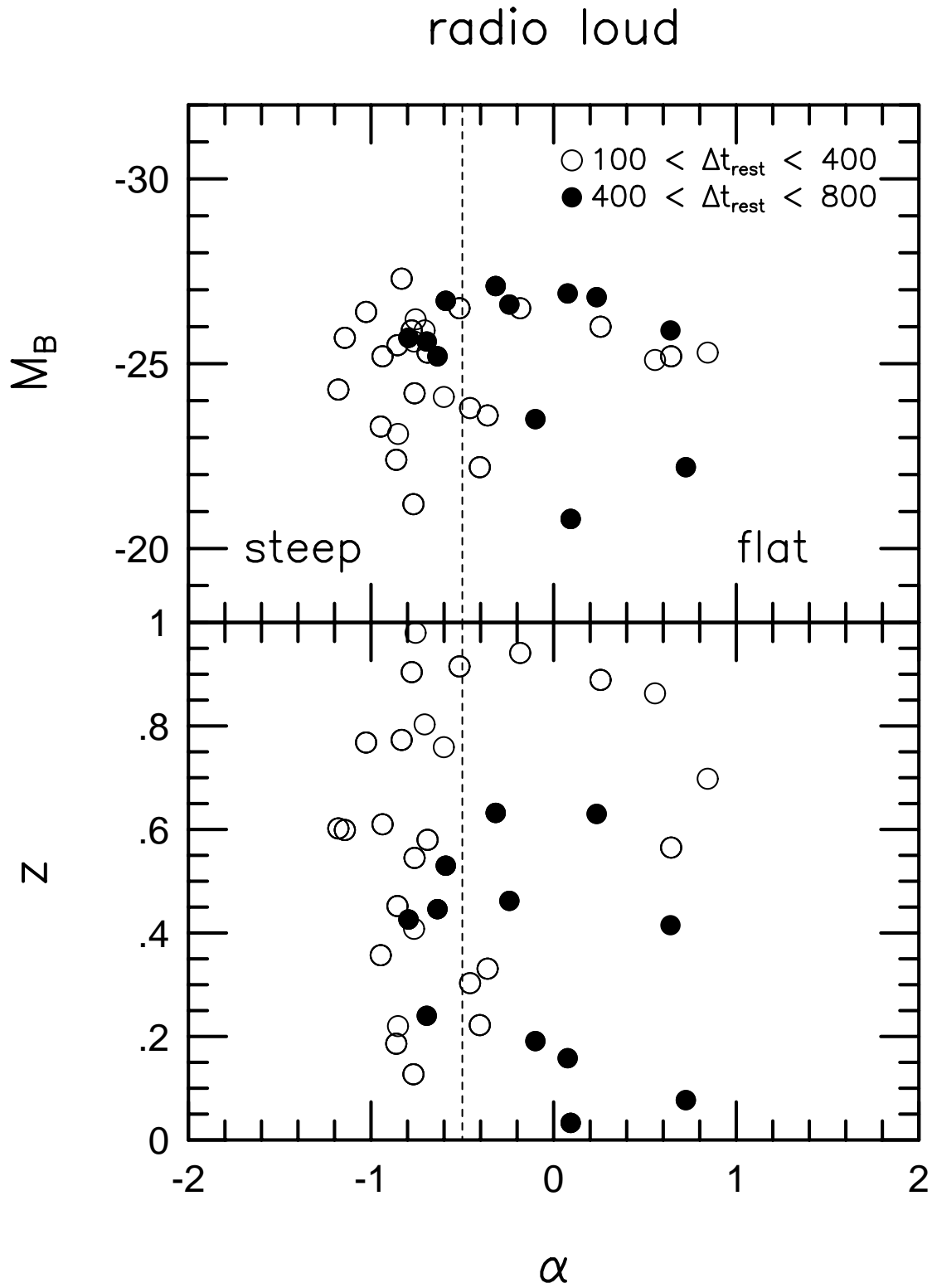


Figure 13

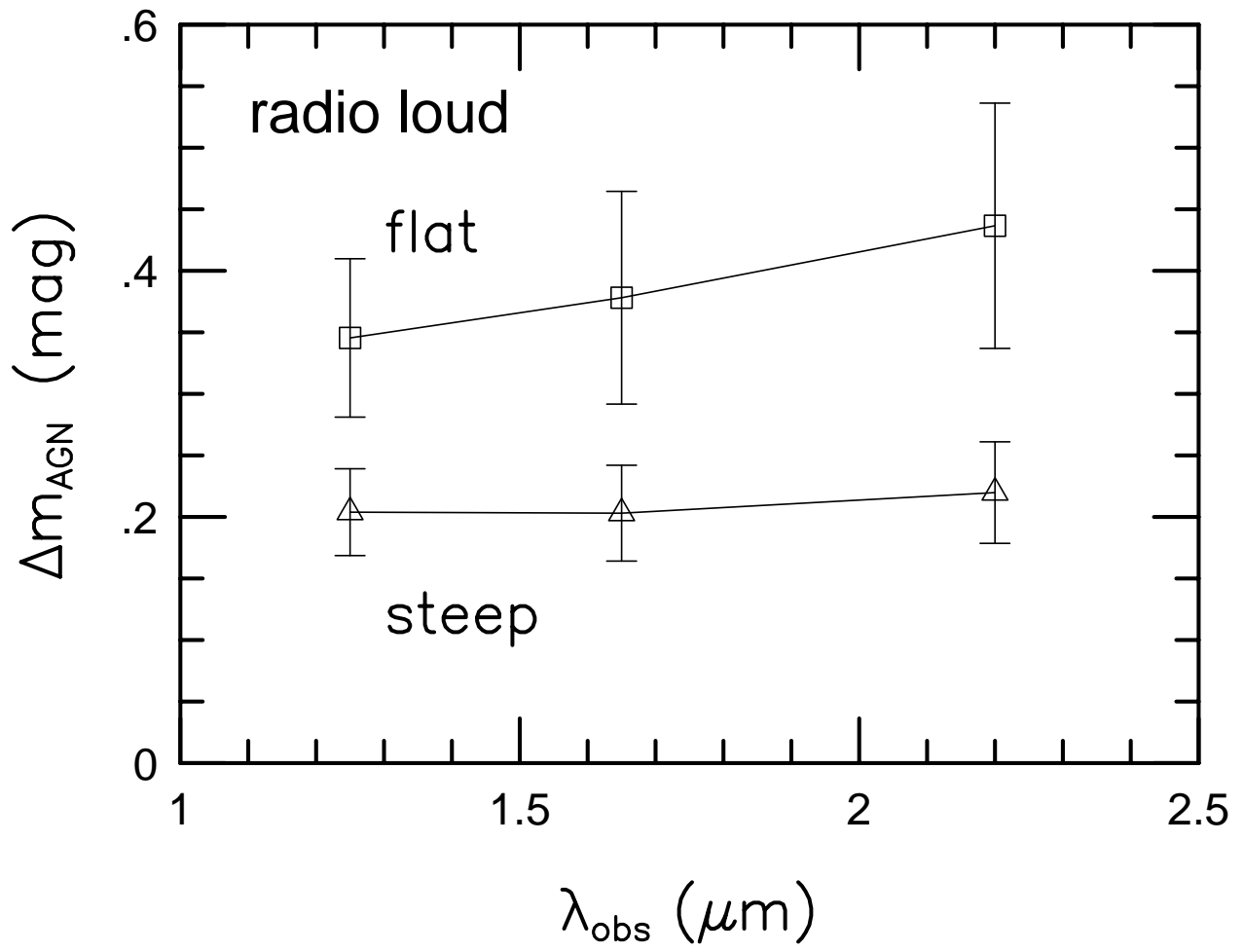


Table 1. Ratio of ensemble variabilities in two groups of AGNs

Tested property	$\Delta m(\text{“}a\text{”})/\Delta m(\text{“}b\text{”})$			
	J	H	K'	Average
Radio strength	1.37	1.37	1.65	1.46
Δt_{rest}	1.22	1.37	1.14	1.24
M_B	1.29	1.18	1.14	1.20
Redshift	1.05	0.95	1.16	1.05
Seyfert type	1.06	1.04	0.92	1.01
$J-H$	1.02	1.00	1.01	1.01
$H-K'$	1.25	1.07	0.99	1.10

Note. — The entire sample is divided by each parameter into the “ a ” and “ b ” groups, such as ($f_\nu(6\text{cm})/f_\nu(V) > 100$, $f_\nu(6\text{cm})/f_\nu(V) < 10$), ($400 < \Delta t_{\text{rest}} < 800$, $100 < \Delta t_{\text{rest}} < 400$), ($M_B < -23.5$, $M_B > -23.5$), ($0 < z < 0.3$, $z > 0.3$), (Seyfert 1–1.5, Seyfert 1.8–2), ($J-H < 0.8$, $J-H > 0.8$), and ($H-K' < 0.8$, $H-K' > 0.8$).

Table 2. Test for wavelength dependence of the ensemble variability

Sample	a_1	a_2	Confidence interval of a_2	
			95%	99%
All AGNs	0.205	0.029	-0.192 – 0.242	-0.248 – 0.295
Radio-quiet AGNs	0.205	-0.065	-0.333 – 0.193	-0.403 – 0.258
Short Δt_{rest}	0.139	-0.044	-0.575 – 0.452	-0.741 – 0.593
Long Δt_{rest}	0.242	-0.079	-0.404 – 0.234	-0.494 – 0.316
Radio-loud AGNs	0.213	0.136	-0.342 – 0.582	-0.470 – 0.693
Short Δt_{rest}	0.190	0.169	-0.398 – 0.703	-0.556 – 0.841
Long Δt_{rest}	0.251	0.111	-0.952 – 0.992	-1.313 – 1.228

Note. — The test was done by adopting a two-parameter function of $\Delta m_\lambda = a_1 \exp(a_2 \lambda)$.

Table 3. Test for radio strength, Δt_{rest} , M_B , and z dependence of the ensemble variability

Sample	Tested property	a_1	σ_{a_1}	χ^2	$P(\%)$
All AGNs	Radio strength	0.196	0.007	15.767	>99.9
Radio-quiet AGNs	Δt_{rest}	0.167	0.008	27.797	>99.9
Short Δt_{rest}	M_B	0.126	0.011	2.757	75.0
.....	z	0.115	0.010	6.179	95.5
Long Δt_{rest}	M_B	0.212	0.012	1.167	44.0
.....	z	0.196	0.011	14.692	>99.9
Radio-loud AGNs	Δt_{rest}	0.262	0.019	1.125	71.1
Short Δt_{rest}	M_B	0.131	0.016	35.898	>99.9
.....	z	0.117	0.013	39.503	>99.9

Note. — P represents the reliability of rejecting the hypothesis that $\Delta m_\lambda = a_1$ does not depend on the tested property.

Table 4. Correlation coefficient r_{ij} of variabilities in the λ_i and λ_j bands

Sample	λ_i, λ_j	n	r_{ij}	Confidence interval (68.3%)
All AGNs	J, H	127	0.74	0.70 – 0.78
.....	H, K'	111	0.81	0.77 – 0.84
.....	J, K'	118	0.71	0.66 – 0.76
Radio-quiet AGNs	J, H	91	0.65	0.59 – 0.71
.....	H, K'	84	0.72	0.66 – 0.77
.....	J, K'	85	0.65	0.59 – 0.71
Radio-loud AGNs	J, H	31	0.88	0.83 – 0.91
.....	H, K'	24	0.91	0.87 – 0.94
.....	J, K'	30	0.86	0.80 – 0.90

Note. — n represents the number of AGNs in a sample.

Table 5. Equivalence test for the correlation coefficients r_{JH} , $r_{HK'}$, and $r_{JK'}$

Sample	r_{JH}	$r_{HK'}$	$r_{JK'}$	r_{true}	$P(\%)$
Radio-quiet AGNs					
$z = 0.0 - 0.1$	0.69 (36)	0.77 (38)	0.77 (38)	0.75	31.5
$z = 0.1 - 0.3$	0.63 (29)	0.89 (23)	0.57 (22)	0.72 ¹	96.8
$z = 0.3 - 0.6$	0.65 (19)	-0.04 (17)	0.50 (19)	0.42	58.1
$z = 0.6 - 1.0$	0.52 (7)	-0.51 (6)	-0.11 (6)	0.03	68.3
Radio-loud AGNs					
$z = 0.1 - 0.3$	0.74 (6)	0.76 (5)	0.04 (5)	0.60	46.0
$z = 0.3 - 0.6$	0.70 (10)	0.67 (8)	0.72 (11)	0.70	1.17
$z = 0.6 - 1.0$	0.94 (12)	0.97 (9)	0.95 (12)	0.95	12.9

Note. — The number in the parentheses is the number of AGNs in a sample. r_{true} is the estimation of true correlation coefficient. P is the reliability of rejecting the hypothesis that r_{JH} , $r_{HK'}$, and $r_{JK'}$ are equivalent to each other.

1: The value of $r_{\text{true}} = 0.72$ is not adequate since the equivalence is rejected.

Table 6a. Fitted values of the parameters in a function of $\Delta m = A(\Delta t_{\text{rest}})^p$

Sample	A	p	Confidence interval of p	
			95%	99%
All AGNs	0.044	0.26	– 0.53	– 0.60
Radio-quiet AGNs	0.0036	0.63	0.30 – 1.00	0.22 – 1.09
Radio-loud AGNs	0.077	0.21	– 0.79	– 0.91

Note. — The cases with no lower limit to the confidence interval are those for which the lower limit becomes negative.

Table 6b. Fitted values of the parameters in a function of $\Delta m = B(1 - \exp(-\Delta t_{\text{rest}}/\tau))$

Sample	B	τ	Confidence interval of τ	
			95%	99%
All AGNs	0.24	180	50 – 370	– 440
Radio-quiet AGNs	0.30	510	200 –	170 –
Radio-loud AGNs	0.29	140	– 820	– 2040

Note. — The cases with no lower limit to the confidence interval are those for which the lower limit becomes negative. The cases with no upper limit are those for which linear relation of $\Delta m \propto \Delta t_{\text{rest}}$ is accepted from the χ^2 test.

Table 7. AGNs in the literature which support a dust reverberation model.

Object	Ref	z	M_B	$f_\nu(6\text{cm})/f_\nu(V)$
GQ COM	1	0.165	-24.4	0.0
Fairall 9	2	0.046	-23.0	0.0
NGC 3783	3	0.009	-19.7	0.7
MARK 744	4	0.010	-19.3	0.0
NGC 4151	5	0.003	-18.7	2.3
NGC 1566	6	0.004	-18.0	3.7

Note. — The data of z , M_B , $f_\nu(6\text{cm})$, and $f_\nu(V)$ are taken from the VV catalog. All AGNs listed here are regarded as radio quiet satisfying our criterion of $f_\nu(6\text{cm})/f_\nu(V) < 10$.

References: (1) Sitko, M. L. et al. 1993, (2) Clavel, J., Wamstecker, W. and Glass, I. S. 1989, (3) Glass, I. S. 1992, (4) Nelson, B. O. 1996b, (5) Oknyanskii, V. L. 1993, (6) Baribaud, T. et al. 1992.

Table 8. Statistics of AGNs based on Nelson’s V and K band monitoring observations.

Sample	Number of AGNs in a sample		
	Radio quiet	Radio loud	Ambiguous
All AGNs	43	5	3
AGNs with detected variability ¹	29	3	1
AGNs with time delay obtained ²	6	0	0

Note. — The result of variability and time delay is taken from Nelson (1996a).

1: AGNs for which the variability is detected in either V or K band or in both.

2: AGNs for which the variability is detected in both V and K bands and the time delay of light variation in the K band relative to the V band is measured.